Lab on a Chip

ELECTRONIC SUPPLEMENTARY INFORMATION

Acoustofluidic particle manipulation inside a sessile droplet: four distinct regimes of particle concentration

Ghulam Destgeer, Hyunjun Cho, Byung Hang Ha, Jin Ho Jung, Jinsoo Park, and Hyung Jin Sung*

Numerical simulation

Simulations on the flow inside the droplet subjected to SAW were performed. An axisymmetric water droplet on the piezoelectric substrate with a contact angle of 90° (hemisphere) was used as the computational domain. Following the work of Alghane *et al*. [Ref. 35-37], the liquid-solid interface was assigned to a no-slip condition, and the liquid-air interface was assumed to be a slip boundary without deformation. The flow was driven by a body force which represents the effects of the leaky SAW [Ref. 59] as

$$F_r = \rho_f(1+\alpha_1^2)A^2\omega^2 k_i \exp(2k_i r + 2\alpha_1 k_i z),$$

and

$$F_z = \rho_f(1+\alpha_1^2)A^2\omega^2 k_i \alpha_1 \exp(2k_i r + 2\alpha_1 k_i z),$$

where $\alpha_1 = j\alpha$ denotes the complex conjugate of the attenuation constant α given by

$$\alpha = \left[1 - \left(c_s/c_f\right)^2\right]^{1/2},$$

and $\omega = 2\pi f$ is the angular frequency, and k_i the complex component of the SAW number $k_L = k_r + jk_i$.

The physical properties of water and the piezoelectric substrate at room temperature were used, and the effects of the gravity were neglected. To obtain the asymmetrical behaviour, the overlapping length of the droplet and SAW were controlled to be smaller than the droplet radius, as depicted in Fig. S1. As a result, a single vortex was observed in each case. The central axis of the vortex approached to the centre axis of the droplet as the SAW force grew, which can be achieved from larger SAW amplitude (Fig. S2) and/or longer overlapping length. The effects of the particle were neglected in the simulation, thus the result represent the case with small particles only.

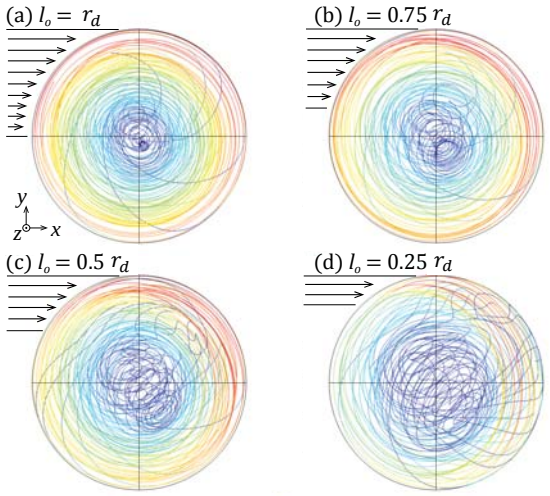

Fig. S1 Simulation results of streamlines showing the effects of the SAW overlapping length at f = 10 MHz. The shape of the vortex structure and velocity distribution became irregular at smaller overlapping length.

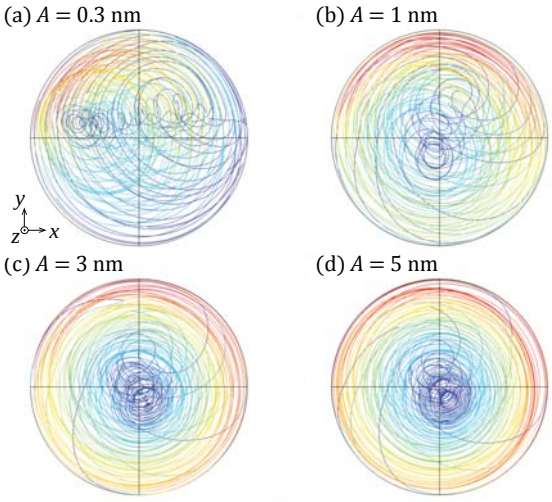

Fig. S2 Simulation results of streamlines showing the effects of the SAW amplitude on the flow inside the droplet at f = 10 MHz. The colour represents the velocity magnitude. The cases (a)-(d) correspond to the SAW amplitudes of 0.3, 1, 3, and 5 nm, respectively. The position of vortex centre varied with the SAW amplitude. At high amplitudes, the vortex centre was fixed at the droplet centre.

Department of Mechanical Engineering, KAIST, Daejeon 34141, Korea.
**Email: hjsung@kaist.ac.kr, Tel: +82-42-350-3027, Fax: +82-42-350-5027*
Electronic Supplementary Information (ESI) available: Additional results and experimental details.

Experimental

Fabrication process

The fabrication process for the acoustofluidic devices used in this study is simpler than the polydimethylsiloxane (PDMS) microfluidic channel based acoustofluidic devices. The present devices does not necessitate any closed chamber or channel for their operation, therefore, we can fabricate the device using a piezoelectric platform without fabricating and bonding a separate PDMS structure. A piezoelectric substrate made of lithium niobate (128 degree Y-cut X-propagating $LiNbO_3$, MTI Korea) with 500 μm thickness is used as a platform to deposit metal electrodes on top. A pair of comb shaped, uniformly spaced metal (Cr/Au, 300/1000 Å) electrodes are deposited (using e-beam evaporation and lift-off processes) on top of $LiNbO_3$ substrate to make an interdigitated transducer (IDT). The width of the electrodes and the spacing between them are set equal to 1/4 of the wavelength of the surface acoustic wave (SAW) such that the SAW frequency matches with the frequency of the input alternating current (AC) signal. The SAW is a type of Rayleigh wave for which most of the acoustic energy is concentrated on the substrate surface. The frequency of the SAW is estimated by dividing the speed of sound on the piezoelectric substrate surface (corresponding to Rayleigh wave mode) to the SAW wavelength (defined by the inter-electrodes spacing). Connecting wires are attached to the metal electrodes of the IDT using a soldering gun and female SMA connector is attached to the opposite sides of the wires.

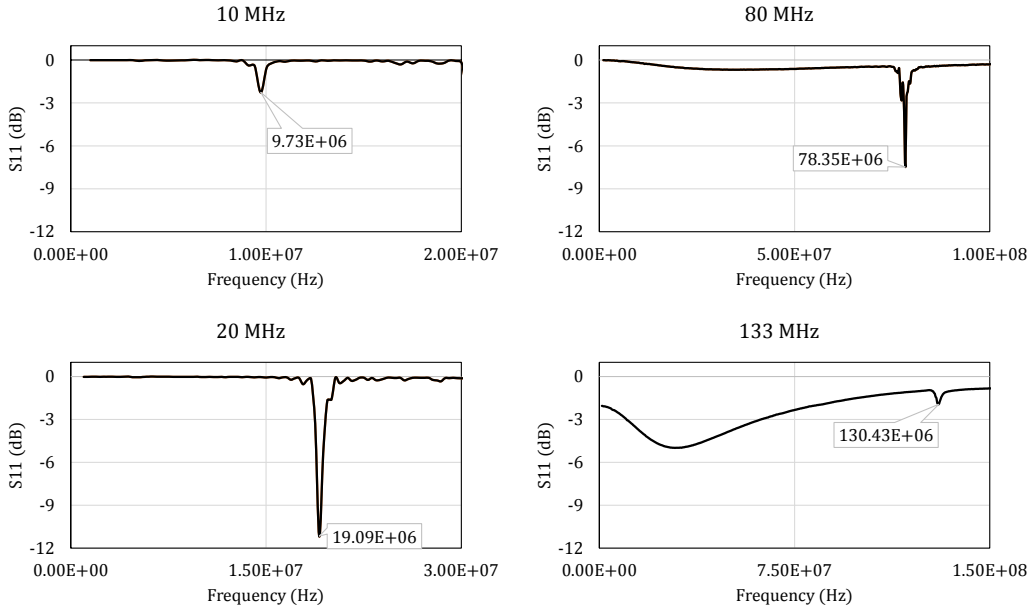

Fig. S3 S11 parameter obtained for four different types of devices operating at the nominal frequencies 10, 20, 80 and 133 MHz, respectively.

Device operation

To measure the resonant or ideal actuation frequency of the device, S11 parameters are estimated using a network analyser (Agilent Technologies (Keysight), USA). The S11 parameter (voltage reflection coefficient) value estimates the electrical power that is reflected from the device in comparison with the power transmitted to the device. A minimum S11 value means that the power reflection is the least that ensures maximum power transmission to the device. The S11 parameters obtained for a single port system for different devices are plotted in Fig. S3. To operate an acoustofluidic device for experimentation, an AC signal is produced by a radio frequency (RF) signal generator (N5181A, Agilent Technologies (Keysight), USA) and amplified using a power amplifier (LZY-22+, Mini Circuits, USA) before feeding the signal into the device. The frequency of the AC signal is tuned to match well with the frequency value obtained from the S11 parameter plot to ensure maximum energy transfer to the device.

Sample preparation

The sample fluid is prepared by mixing polystyrene (PS) particles having required diameter with deionized (DI) water (OCI, Korea). The nominal diameters of different types of PS particles are used, range from 1 μm to 30 μm. For simplicity, we have used nominal diameter values for the particles in the manuscript. Two kinds of particles are used, non-fluorescent dyed particles and fluorescent particles. The dyed particles include 1 μm (Polybead® polystyrene black dyed 1.00 micron microspheres, 2.6% solid-latex, mean diameter (MD) 1 μm, standard deviation (SD) 0.03 μm, coefficient of variation (CV) 3%, catalogue number (CN) 24287, Polysciences, Inc.), 6 μm (Polybead® polystyrene yellow dyed 6.0 micron microspheres, 2.7% solid-latex, MD 5.8 μm, SD 0.177 μm, CN 15716, Polysciences, Inc.), and 10 μm (Polybead® polystyrene violet dyed 10.0 micron

microspheres, 2.6% solid-latex, MD 9.9 μm, SD 0.494 μm, CN 18139, Polysciences, Inc.) diameter particles. The fluorescent particles include 1 μm (Polymer microspheres, red fluorescing, 1% solid, MD 1.0 μm, CN R0100, Duke Scientific Corp.), 3 μm (Fluoro-Max™ red fluorescent polymer microspheres, 1% solid, MD 3.2 μm, CN R0300, Thermo Scientific), 5 μm (Fluoro-Max™ green fluorescent polymer microspheres, 1% solid, MD 4.8 μm, CN G0500, Thermo Scientific), 10 μ m (Fluoro-Max™ green fluorescent polymer microspheres, 1% solid, MD 9.9 μm, CN G1000, Thermo Scientific), and 30 μ m (Fluoro-Max™ red fluorescent polymer microspheres, MD 31 μm, CV 8.4%, CN 36-6B, Thermo Scientific) diameter particles.

Image acquisition and analysis

The experiments are conducted on the stage of fluorescent microscope (BX53, Olympus, Korea) equipped with a camera (DP72, Olympus, Korea) to record the results. For fluorescent imaging, the built-in light source and filters in the microscope are used to acquire the images, however, for capturing images of the dyed particles, an external light source (Mckinley Q5, LED flash light) attached to a stand is used to shine light on the water sessile droplet from the top at an angle. However, a piece of white paper is attached to the bottom of the substrate (for double side polished) to enhance visibility of the particles. Such a light source configuration produces shadows of the droplets and particles on the paper surface underneath the substrate which is visible in some of the experimental demonstrations. The images captured using the camera are processed and analysed using an open source image processing software (ImageJ, http://imagej.nih.gov/ij/).

Results

For brevity purpose, we have included limited figures in the main manuscript, however, to further enhance the understanding of the phenomenon, additional results on four different regimes (R1-R4) of particle concentration are presented here. The gradual concentration of 6 μm particles at the centre of droplet in Fig. S4 is a demonstration of R1. Figures S5 shows the time lapse images corresponding to R3. Mixed regime configurations are demonstrated in Fig. S6 ((a) R1 and R3, (b) R2 and R4), where different pairs of particles are separated. Figure S7 demonstrate R1 and R2 using 10 MHz SAWs. Figure S8 shows separation of fluorescent particles and image stacking procedure.

Caption to ESI Movie I

Four distinct regimes (R1-R4) of particle concentration, corresponding to C20-6, C10-1, C20-30, and C133-6 (Fig. 4 in the manuscript), are presented in the movie. The separation of 1 and 10 μ m particles, corresponding to Fig. 6(a-b) in the manuscript, is also demonstrated.

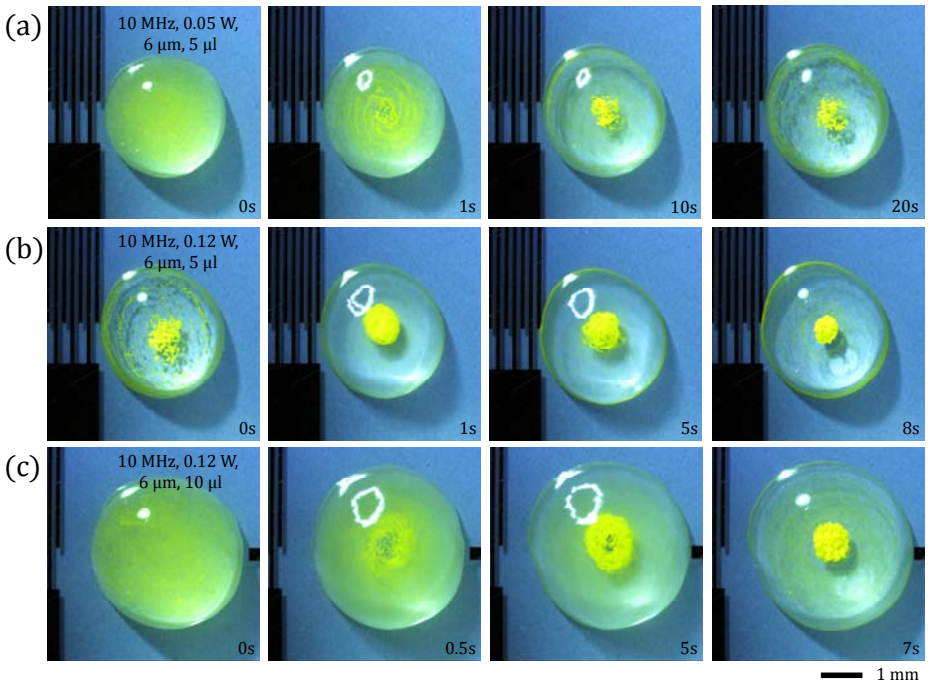

Fig. S4 (a) Concentration of 6 μm particles inside a 5 μl water droplet is demonstrated (R1). The formation of standing acoustic waves is quite visible that drives the particles towards the centre of droplet along with the acoustic streaming flow in the clockwise direction. (b) The input power is increased from 0.05 W to 0.12 W that results in immediate clustering of the particle at the centre. The patterns of particles under the influence of the standing waves also disappear. (c) The concentration of particles in a 10 μl droplet of water is demonstrated.

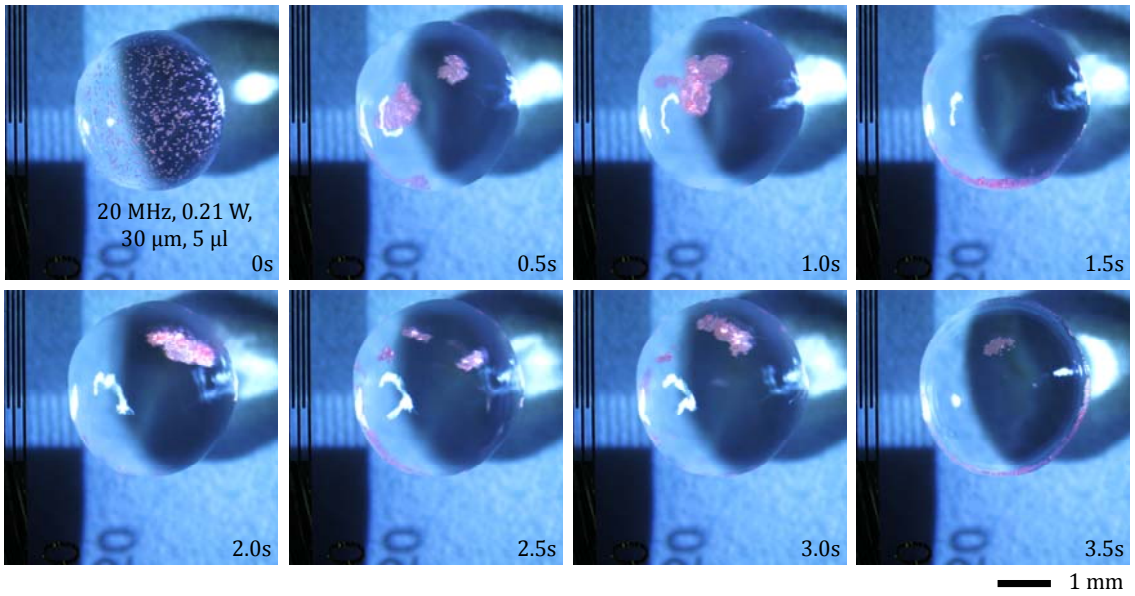

Fig. S5 Particle concentration on the side of water drop is shown (R3). A tug of war takes place between the ARF by the travelling and standing wave and the ASF drag force. The particles are clustered under the influence of standing waves and then driven towards the side of the droplet by the ASF and the ARF from traveling SAWs.

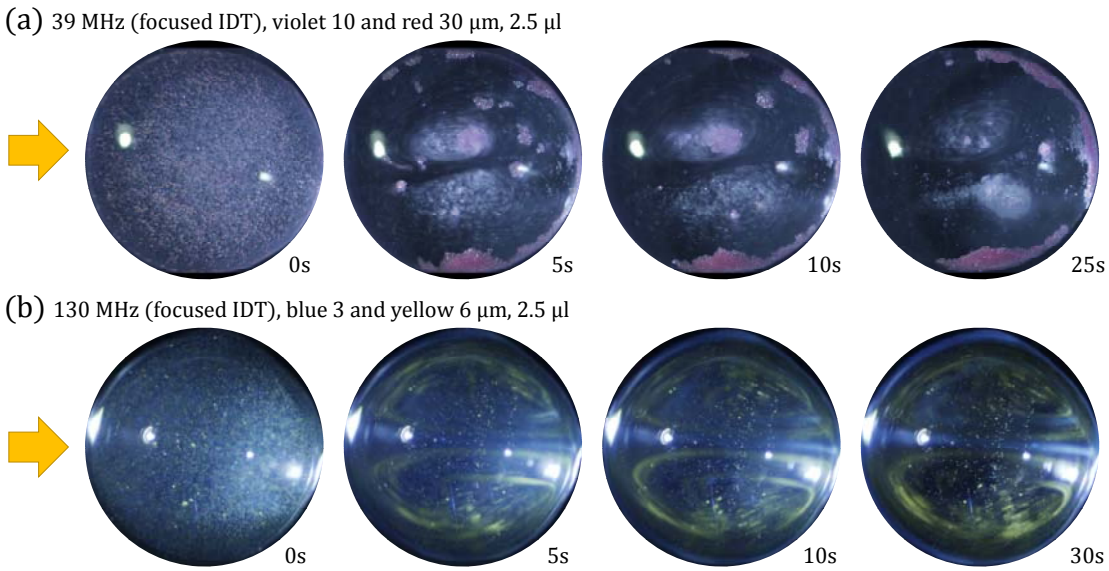

Fig. S6 Manipulation of particles using focused interdigitated transducers (operating at 39 and 130 MHz frequencies) is demonstrated. (a) For focused 39 MHz SAWs, the larger particles red 30 μm in diameter are gradually pushed to the side of the droplet (R3), whereas the smaller dyed violet 10 μm particles are concentrated at the centres of the ASF vortices (R1). The separation of the particles (10 and 30 µm) is apparent. Similarly, polystyrene particles 3 μm (dyed blue) and 6 μm (dyed yellow) are separated using focused 130 MHz SAWs. The smaller particles (3 μm) move away from the ASF vortex (R2), whereas the larger particles (6 μm) form smaller particle ring structure close to the vortex centre (R4).

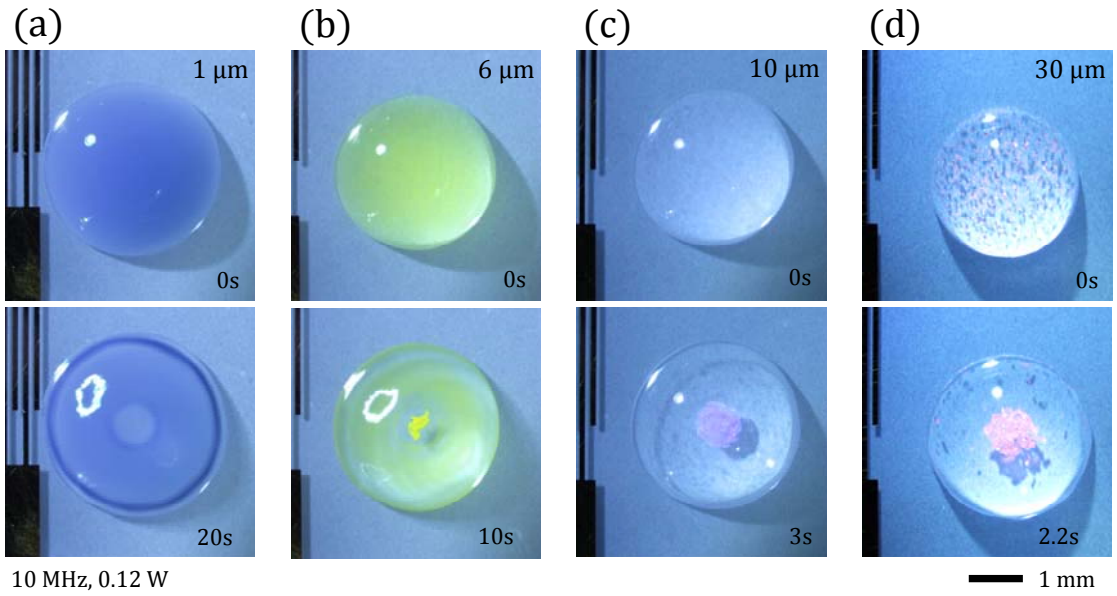

Fig. S7 Temporal progression of particle concentration is shown under 10 MHz SAWs with 0.12 W power input for polystyrene particles having diameter (a) 1 μm, (b) 6 μm, (c) 10 μm, and (d) 30 μm. Figure (a) corresponds to regime R2 of particle concentration in the form of a ring, while (b-d) corresponds to regime R1. It is evident that the particles concentration at the centre of the droplet becomes rapid with increase in particle diameter from (b) to (d).

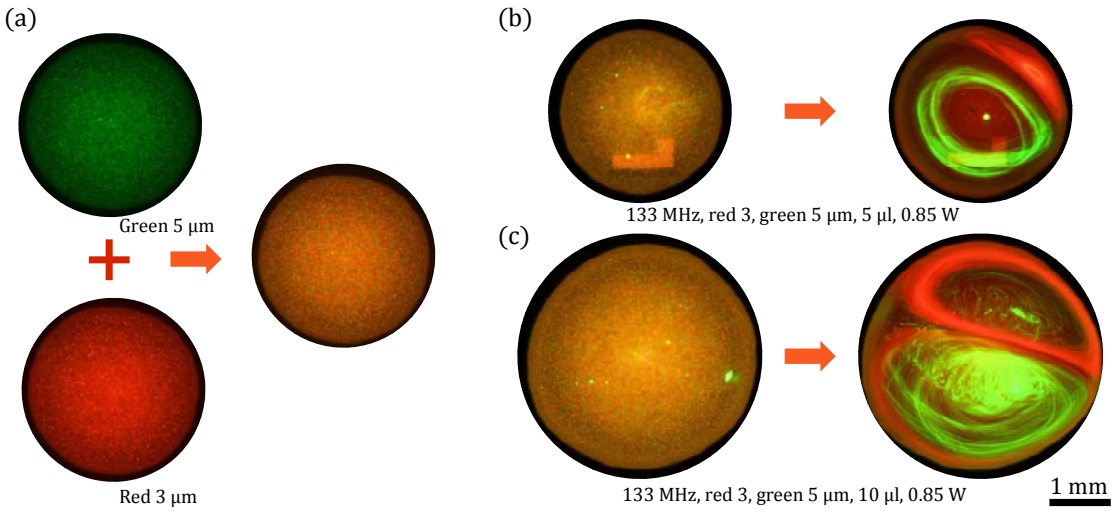

Fig. S8 Fluorescent particles (red and green) are suspended together inside the water droplet to realize particle separation, however, the images are captured separately using appropriate filters. (a) Therefore, two images are stacked together to obtain a common image showing the red and green particles in a single frame. (b) Separation of red 3 and green 5 μm particles inside a 5 μl droplet is demonstrated (R2 and R4). (c) Further, separation of particle is also demonstrated inside a 10 μl droplet.